SAND2022-13956J

Dynamics of the gold-silicon eutectic reaction studied at limited length scales using *in situ* TEM and STEM

Sandra Stangebye[1,2], Changhui Lei[3], Aubri Kinghorn[1], Ian Robertson[3,4], Josh Kacher[2,3], Khalid Hattar[1,3]

[1] Sandia National Laboratories, Albuquerque, New Mexico 87185, USA

[2] School of Materials Science and Engineering, Georgia Institute of Technology, Atlanta, Georgia 30332, USA

[3] Department of Materials Science and Engineering, University of Illinois Urbana-Champaign, Urbana, Illinois 61801, USA

[4] Department of Materials Science and Engineering, University of Wisconsin-Madison, Madison, Wisconsin 53706, USA

Corresponding Author: Sandra Stangebye (sstangebye3@gatech.edu)

Author's ORCID:

Sandra Stangebye (0000-0002-7811-1769)
Ian Robertson (0000-0002-4923-0400)
Josh Kacher (0000-0003-0304-3367)
Khalid Hattar (0000-0002-0609-2802)

Abstract

The dynamics of the gold-silicon eutectic reaction in limited dimensions were studied using *in situ* transmission electron microscopy and scanning transmission electron microscopy heating experiments. The phase transformation, viewed in both plan-view and cross-section of the film, occurs through a complex combination of dislocation and grain boundary motion and diffusion of silicon along gold grain boundaries, which results in a dramatic change in the microstructure of the film. The conversion observed in cross-section shows that the eutectic mixture forms at the Au-Si interface and proceeds into the Au film at a discontinuous growth rate. This complex process can lead to a variety of microstructures depending on sample geometry, heating temperature, and the ratio of gold to silicon which was found to have the largest impact on the eutectic microstructure. The eutectic morphology varied from dendrites to hollow rectangular structures to Au-Si eutectic agglomerates with increasing silicon to gold ratio.

Keywords: Au, Silicon, eutectic reaction, phase transformation, transmission electron microscopy (TEM), scanning transmission electron microscopy (STEM)

1. Introduction

Gold (Au) and silicon (Si) are often used together in integrated circuit (IC) and microelectromechanical (MEMS) manufacturing and have been a key in creating complicated designs due to their respective properties [1]. In particular, the Au-Si eutectic reaction is used in the packaging stage of MEMS device fabrication because of the mechanical strength and hermicity of the eutectic bond [2–4]. However, both of these properties are often degraded by poor bonding, though the microstructural and environmental factors dictating the bonding behavior have not been well established. Additionally, the current IC technology node scales down to just a few nanometers [5], which requires precise understanding and control of the materials being used at such limited length scales. Further study of this eutectic reaction is necessary to address commercial concerns, develop new applications, and determine the fundamental physics of the eutectic reaction at limited length scales.

The thermodynamics of the Au-Si eutectic reaction is described by a simple eutectic phase diagram with a eutectic temperature of 636 K and concentration of 18.6 at% Si [6]. The two elements show negligible solubility in other phases. However, at least 12 metastable phases ranging from fractional ratios, such as $Au_{.81}Si_{.19}$, to Au_3Si have been reportedly produced by a wide variety of methods [7–12], with crystal structures including face-centered cubic (FCC) [13], cubic [7,11,12], hexagonal [10], and orthorhombic [8,9,14].

During the eutectic reaction, it is generally accepted that a liquidous Au-Si mixture forms and, upon solidifying, creates the eutectic bond. However, there are discrepancies reported in the literature regarding the exact mechanisms in which the eutectic bond forms. There are reports that Au diffuses into Si during the eutectic reaction [8,15,16], with some reports suggesting that this occurs even at temperatures below the eutectic point for electron transparent samples [8,15]. This was recently documented by Terauchi *et al.* via *in situ* transmission electron microscope (TEM) heating experiments that showed Au diffusion into a Si substrate at 533 K [15]. Other reports have shown that the early diffusion of Au into Si can lead to gold silicide formation prior to the eutectic temperature [8]. This is contrary to other studies that show the eutectic mixture does not form until the temperature has reached the eutectic point [17]. It is important to note that the reports of Au diffusion prior to the eutectic temperature occurred in electron transparent samples. This could indicate that the observed pre-eutectic Au diffusion is a thin-film effect and likely does not occur in bulk materials. There are also multiple reports that Si diffuses into Au as evident by silicon oxide formation on the surface of the Au film [18–21].

Several authors have reported on the strong role played by the Au grain boundaries in the fast diffusion of Si

[14,20,22,23]. Specifically, Seibt *et al.* observed that high angle Au grain boundaries served as preferential nucleation sites for gold silicide, which exhibited an epitaxial relationship with the neighboring Au grains [23]. This suggests that forming low-energy interfaces is an important factor during the formation of the eutectic bond.

Complicated final microstructures ranging from nanowires [24,25] to fractals [26] have been reportedly formed via reactions at the Au-Si interface at elevated temperatures. Dendritic structures, square shaped particles, and rectangular pores have also been reported [16,27,28]. Philofsky *et al.* found that the final microstructure resulting from the eutectic reaction was a function of cooling rate and Si orientation [29]. This was later confirmed by Kato *et al.* with the observation that Au dendrite size decreased with increasing Au-Si cooling rate and that both the dendrite texture and squared Si growth were influenced by Si orientation [28].

It remains unclear how the initial microstructure, sample geometry, and bonding conditions may influence the bonding microstructure and the overall behavior of the eutectic bond. The present study provides a detailed analysis of the dynamics of the Au-Si eutectic reaction occurring at limited dimensions observed via *in situ* TEM and scanning transmission electron microscopy (STEM) heating. This includes the observation of relaxation and recrystallization of the Au film prior to the eutectic reaction, Si diffusion along Au grain boundaries, and a detailed characterization of eutectic bond microstructure.

2. Results

a. Initial Microstructure of Au films

The sample fabrication produced well-adhered Au thin films with nanocrystalline grains. An example of the grain structure for a 200 nm-thick plan-view film and the companion histogram of the grain size distribution are presented in **Fig. 1**a and **Fig**. **1**b, respectively. Grain sizes were determined to be the diameter of a circle of equivalent area as the area of each grain. Grain sizes ranged in diameter from 11 nm to 163 nm with an average grain size of 65 nm (arrowed). The grain sizes and microstructures for the microfabricated samples were similar to that of the plan-view. The mean surface roughness of the film was determined using atomic force profilometry to be 2.4 nm. The films had a generally columnar structure, but imaging of cross-sectional samples revealed that not all the grains extend through the full thickness. Electron diffraction confirmed the dominant expected <111> texture. The film contained structural defects including grain boundaries and intragranular lattice dislocations.

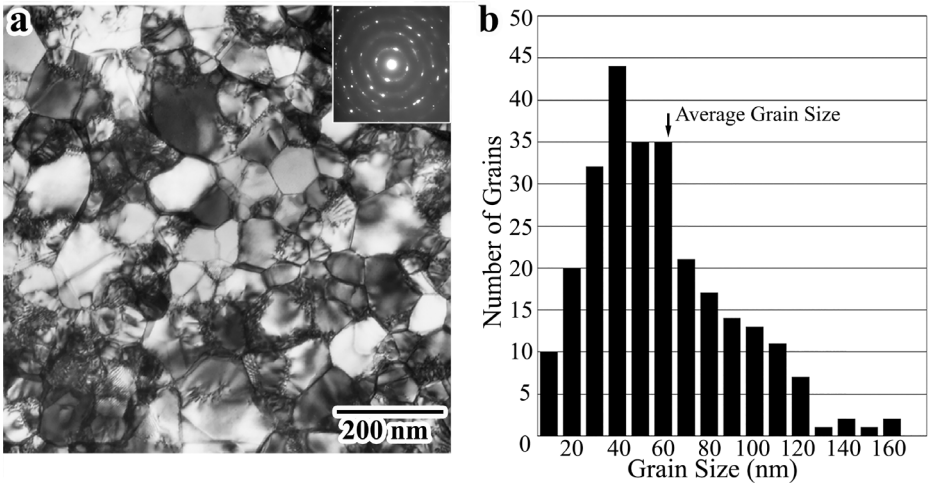

Fig. 1 (a) TEM micrograph of the as-deposited nanocrystalline microstructure of 200 nm-thick plan-view gold film (insert shows characteristic diffraction rings of <111> film texture), (b) histogram displaying the grain size distribution of as-deposited microstructure

b. Eutectic reaction dynamics

The dynamics of the Au-Si eutectic reaction at limited dimensions was elucidated through *in situ* TEM annealing experiments of a set of plan-view and cross-section samples with the geometry and initial microstructures described in the Methods section (**Fig. 10)** and **Fig. 1**, respectively. The dynamics of the Au-Si eutectic reaction of the thin Au film on a large Si substrate shows many microstructural changes in the film and minimal changes in the substrate.

As the eutectic temperature is approached, the first stage in the transformation involves the removal of lattice dislocations and grain growth within the Au film. This can be seen in **Fig. 2**, which displays a series of images of a plan-view sample captured during an *in situ* TEM heating experiment heated to 723 K. The video of this transition can be seen in Supplementary Video 1. Specifically, **Fig. 2**a shows that the Au grains are now free of dislocations, unlike the initial microstructure shown in **Fig. 1**a. The recovery of the Au film also includes recrystallization observed in the grain growth seen when comparing the initial microstructure (**Fig. 1**a) with **Fig. 2**a. The average grain size has increased from 65 nm to 313 nm after heating to 723 K. The grain growth continues when comparing **Fig. 2**a and **Fig**. **2**b as the temperature is held at 723 K. In order to highlight this grain growth during the first 2.37 s, the grain boundaries have been outlined and superimposed for each successive snapshot. **Fig. 2**k, **Fig**. **2**l, and **Fig**. **2**m are the overlayed grain structure for **Fig. 2**a (black) and **Fig**. **2**b (red), **Fig**. **2**b and **Fig**. **2**c (blue), and **Fig. 2**c and **Fig. 2**d (green), respectively. For the majority of grains, those of larger sizes proceed to grow at the expense of the smaller grains. A clear example of this is indicated by an arrow in **Fig. 2**l where a collection of smaller grains outline in red (from **Fig. 2**b) are consumed by a larger grain (blue). Another example of this can be seen by comparing **Fig. 2**a and

b, where the grain indicated by the arrow marked number 1 is consumed by the larger grain larger grain just above it. The average grain size increases from 313 to 422 nm during the 2.37 s separating **Fig. 2**a and **Fig**. **2**d, resulting in an average grain size increase at a rate of 46 nm s^{-1}. During this process, the eutectic mixture has formed at the Au-Si interface and proceeded along the grain boundaries. This leads to the initial thickening and darkening of the grain boundaries and triple junctions as indicated by arrows in **Fig. 2**e. This process appears to occur for every grain boundary and continues as the grain boundary widths increase, the triple junctions enlarge, and the grains become circular. The transformation of the region indicated by a dashed box in **Fig. 2**g is shown at higher magnification in

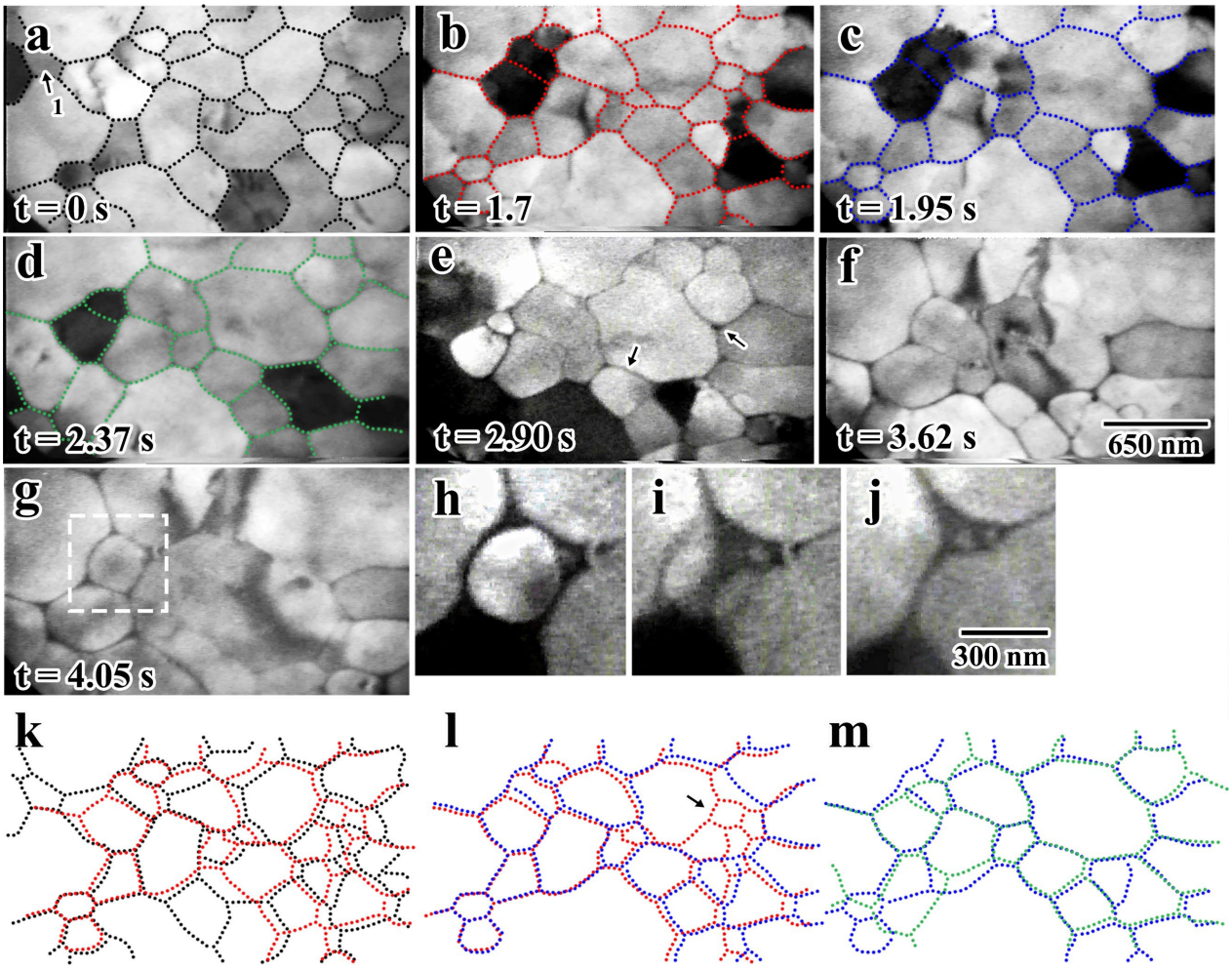

Fig. 2 *In situ* TEM observation of the eutectic reaction in traditional plan-view sample heated above the eutectic temperature to 723 K. (a) Au microstructure after significant recovery including dislocation motion and grain growth (b)–(d) same region after additional grain growth, (e) extensive microstructural changes including widening of the grain boundaries and triple junctions as well as the growth and rounding of the grains (arrows pointing to an example of a widened grain boundary and triple junction), (f)–(g) Au-Si mixture continues to dewet the grain boundaries. (h)–(j) Coalescence of islands occurs during late stages of the eutectic reaction. (h) A small round Au island completely surrounded by liquidous eutectic mixture as indicated by box in Fig. 2g, (i) the Au island mid-transition, (j) the resulting structure that is formed less 0.067s after Fig. 2h due to the consumption of the small island and migration of neighboring larger islands. Overlay of the grain boundary outlines for (k) Fig. 2a-b, (l) Fig. 2b-c, and (m) Fig. 2c-d to show large grains consuming smaller grains.

Fig. 2h-j. The small circular grain in **Fig. 2**h is completely consumed in less than 0.067 s during the transformation and is replaced by a saddle interface structure. During this step (shown in **Fig. 2**i), the grains on either side of the Au island progress approximately 220 nm at a rate of 3.3 μm s^{-1} to result in the final microstructure shown in **Fig. 2**j. This rate is significantly faster than any other microstructural changes documented for this reaction. The full area shown in **Fig. 2**g was converted into a gold silicide just 0.7 seconds after this event occurred.

Further insight into the kinetics of the grain growth and the eutectic transformation was obtained by conducting similar *in situ* TEM heating experiments with cross-sectioned specimens (**Fig. 3)**. The schematic to the left of **Fig. 3**a displays the relative position of Au and Si in the cross-section specimen with the black box indicating the specific location shown by the TEM micrographs. Similar to the plan-view transformation, relaxation is observed in cross-sectional view beginning with the removal of lattice dislocations and grain growth in the Au film. The arrowheads in **Fig. 3**a identify a grain boundary (arrow 1) and intragranular dislocation (arrow 2) present in the initial microstructure. Lattice dislocations in the as-deposited microstructure are removed upon heating just below the eutectic temperature, resulting in the microstructure shown in **Fig. 3**b. This is followed by grain growth in the Au film (**Fig. 3**c). Once the eutectic temperature is reached, the Au-Si liquidous mixture forms at the interface between the Au film and Si substrate (interface indicated by dotted line in **Fig. 3**c). The arrowheads in **Fig. 3**d indicate the Au-Si mixture that has formed at the interface. This mixture progresses along the grain boundaries, converting the boundaries to a Au-Si layer. This leads to the observed widening of grain boundaries as the Au-Si mixture penetrates into the Au grains and transforms it. Simultaneously, the eutectic mixture proceeds into the Au film with an interface of a characteristic meniscus as indicated by arrowheads in **Fig. 3**e and **Fig**. **3**f. The liquidous layer separates the recrystallized grain first from where the initial Au-Si interface region was present, **Fig. 3**e, and then from neighboring grains, **Fig. 3**f. In less than 28 s at 636 K, the entire film has reacted to form a large gold silicide grain, resulting in the microstructure shown in **Fig. 3**h.

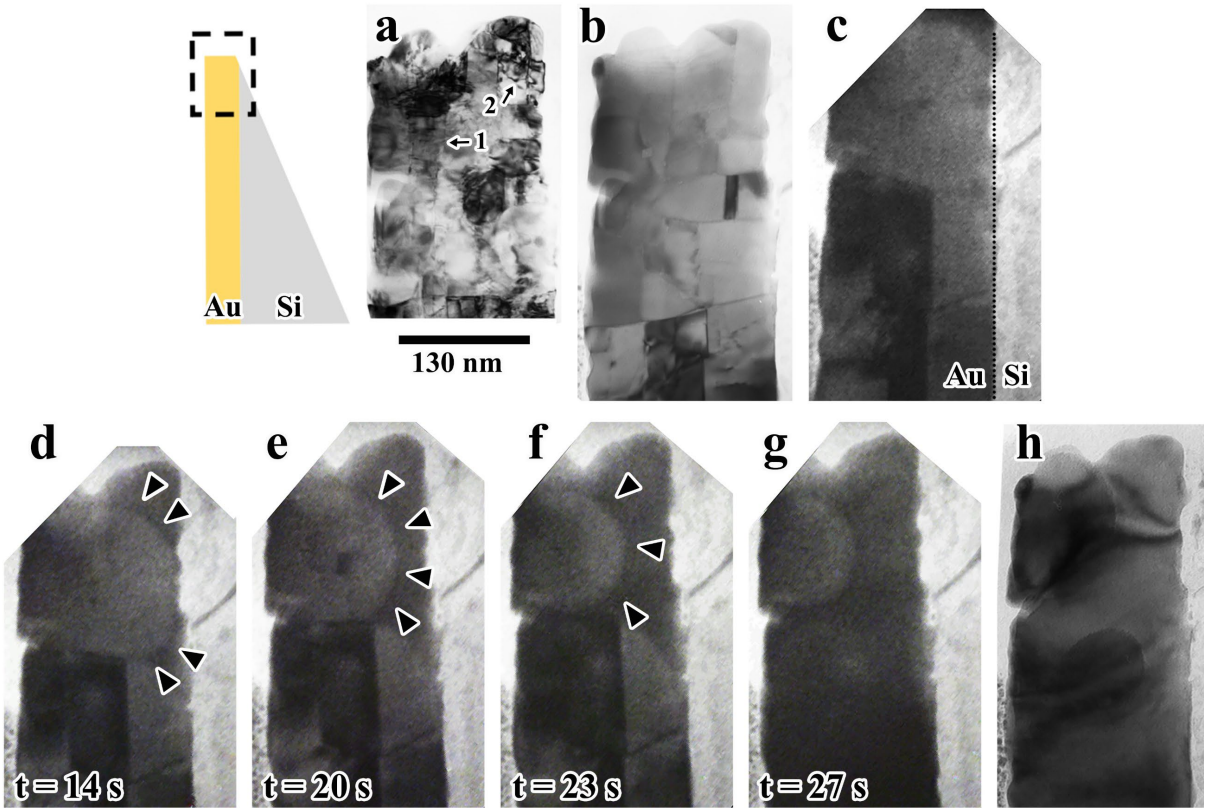

Fig. 3 TEM micrographs of the microstructural evolution observed in cross-section of the Au-Si eutectic reaction. (a) Room temperature as-deposited microstructure containing grain boundaries (arrow 1), and intragranular dislocations (arrow 2) with the schematic of cross-section shown to the left, (b) microstructure free of dislocations and after relaxation, (c) significant grain growth just prior to reaching 636 K (Au-Si interface indicated by the dotted line), (d) initial wetting of interface and grain boundaries after eutectic temperature is reached (arrows point to eutectic mixture that has penetrated from the Au-Si interface), (e) the partial transformation via meniscus migration of gold island. Arrowheads indicate boundary between Au island and liquidous Au-Si mixture, (f)–(g) continued removal of initial microstructure and almost complete transformation of Au film, (h) the final microstructure of the film showing no resemblance to initial microstructure. Time stamps on the micrographs indicate the time elapsed after eutectic temperature was met

The decreasing volume of Au and the changing meniscus curvature of the reaction front are modeled using the projected area to provide a three-dimensional image of the structure, assuming the meniscus is symmetrical with the central axes. The liquid-solid interface progressed at a global rate of 5.4 nm s^{-1}. This rate is significantly slower than the measured rate of the liquidous Au-Si mixture observed in plan-view. The local rate of change can be seen in **Fig. 4**, in which the aerial fraction of remaining Au is plotted as a function of time at 0.33 second intervals. The transformation appears to occur in a discontinuous fashion with periods of rapid conversion followed by periods of stagnation. For example, the region maked '3f' on **Fig. 4** indicates a stagnated period where the percent reacted remains constant for two seconds. This is followed by the region '3g' in which the transformation begins to occur again. Curve fitting each of the regions of increased conversion indicates that the transformation occurs exponentially.

Similar discontinuous behavior has been reported for grain boundary motion in Ni during annealing and has been attributed both to the accumulation of impurity elements at the grain boundaries [30] and the supersaturation of vacancies within grain interiors that halt further boundary progression [31]. In this study, the observed discontinuous behavior is related to the conversion of the Au film during the eutectic reaction, rather than just grain boundary motion. Studies have shown that the growth velocity of the eutectic front depends on the amount of undercooling, with maximum velocity occurring at the maximum undercooling [32,33]. One study also found that varied growth rate of the eutectic front can be attributed to the conversion from anomalous eutectic to slowed growth of 'regular' lamellar eutectic [32]. Considering that this experiment was conducted at a contstant temperature and there was no change in the eutectic morphology, the discontinuous behavior in **Fig. 4** could indicate that diffusion pathways play an important role in the eutectic conversion and that the exhaustion of such pathways lead to stagnation of the conversion.

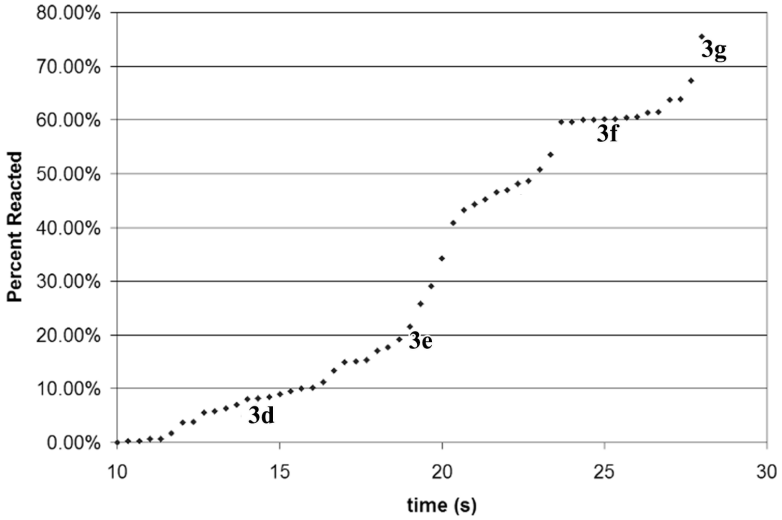

Fig. 4 Graphical representation of the transformation seen in Fig. 3. The x axis is time corresponding to that reported in Fig. 3 and y axis is the aerial percent conversion of the Au island highlighted region in Fig. 3d-g. Note that the growth rate is not uniform.

The diffusion mechanisms operating during the eutectic reaction are shown in greater detail during the *in situ* STEM heating experiment performed under high angle annular dark field (HAADF) STEM imaging conditions, **Fig. 5**. The intensity of HAADF STEM images is roughly proportional to the atomic number squared which creates a stark contrast between the Au and Si [34]. **Fig. 5**a shows the initial microstructure of the cross-sectional sample prior to heating. As the temperature rises to 593 K, observable amounts of Si proceed to diffuse into the grain boundary structures. This leads to the darkening of the grain boundaries in the HAADF STEM images, highlighted in **Fig. 5**b,

as the lighter element Si diffuses into the Au film. Two grain boundaries that show the most extreme darkening and thickening due to Si diffusion are arrowed in **Fig. 5**b. In **Fig. 5**c, complete conversion of the Au film has occurred after the eutectic temperature is met.

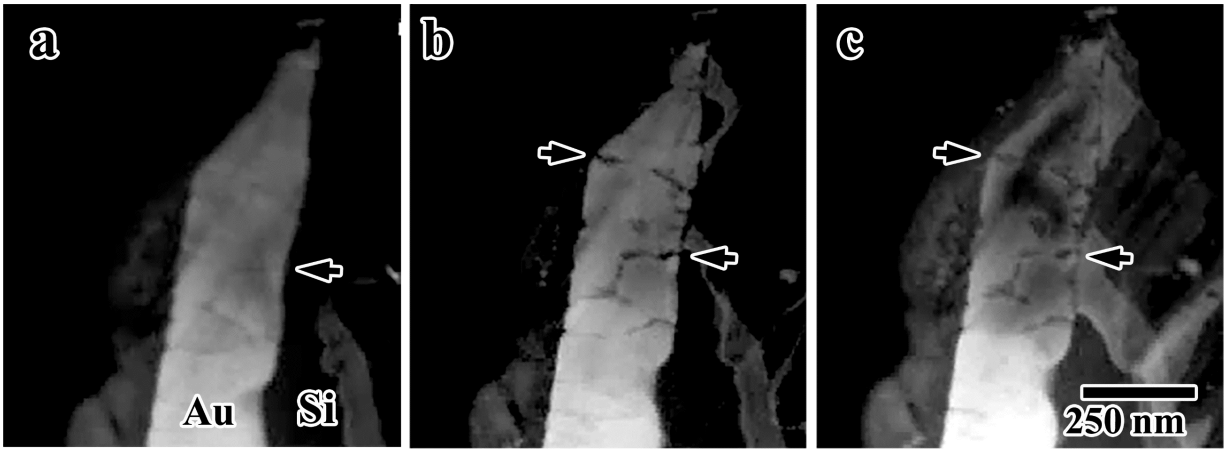

Fig. 5 *In situ* HAADF STEM heating experiment on a cross-sectional Au film on a Si substrate. (a) Room temperature structure of Au film on Si substrate with the location of each indicated and arrow is pointing to a grain boundary. (b) The darkening and widening of the grain boundaries (arrowed) in the Au film as a result of Si diffusion at T = 593 K, (c) the diffusion of Au rich mixtures along the free surface and away from the original film at T = 633 K

c. Post-mortem eutectic structure

Fig. 6 shows analysis of the Au-Si reaction-induced structures after heating a sample to 723 K in the TEM. This experiment was done on a traditional plan-view sample since the wedge shape provided an increasing ratio of substrate (Si) to film (Au) with distance from the edge of the sample (**Fig. 10**a). The Au-Si eutectic reaction at limited length scales resulted in three distinct microstructures that can be correlated to the ratio of Au to Si present in the local regions (labeled A, B, and C in the TEM migrograph **Fig. 6**a). The plan-view experiments reveal that the eutectic mixture eventually completely consumes the Au film and agglomerates on a thin amorphous brittle substrate of very low atomic weight, assumed to be the silicon oxide layer formed on top of the Au thin film due to Si diffusion through the Au film.

Region A, that of the lowest Si concentration, has a structure consisting of coarsened 'fractal-like' dendrites on a silicon oxide layer. Region B contains an intermediate concentration of Si to Au and resulted in the formation of roughly rectangular structures of a few micrometers in width. **Fig. 6**b shows the details of one such structure in which debris is observed within the rectangle and a dark rim is found along the perimeter. Stereomicroscopy performed on this region (specifically on the region shown in **Fig. 6**c) indicated that the Si substrate is banked to form the rectangular structures and that the Au-Si mixture resided on the same side as banked Si faces. This is strong evidence that the Au-

Si debris is residing 'underneath' a thin non-native silicon oxide layer that formed on top of the Au due to Si diffusion through the film. A schematic of the rectangular structure is shown in **Fig. 6**c with each material (Au-Si, Si, and SiO_2) labeled. HAADF imaging, shown in **Fig. 6**d-f, was also performed on the rectangular structures to provide information on the relative locations of Au and Si. This indicated that the debris and rim around the rectangles are a Au-Si mixture, while the region outside of the structure is only Si, which can both be seen in **Fig. 6**e and f, respectively. In the region with the highest Si to Au ratio, Region C, gold silicide was observed to agglomerate into poorly connected islands on the Si surface. It appears, due to the thickness of the Si support, that the silicon oxide film plays a less significant role in the development of these microstructures.

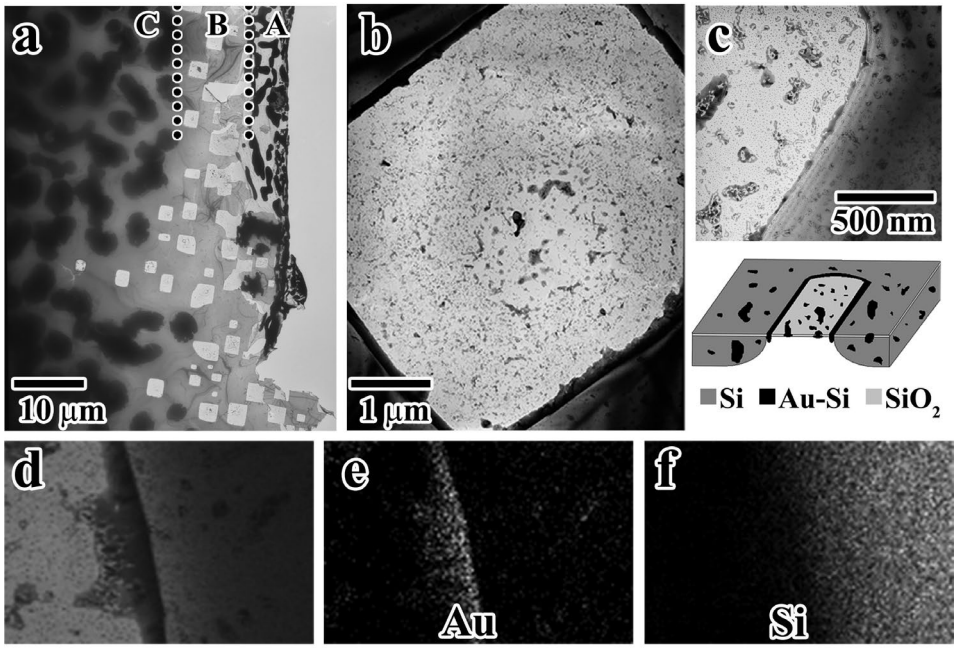

Fig. 6 TEM micrographs of the resulting microstructure of the reaction in plan-view observed in Fig. 2 where the sample was heated to 732 K for less than 120 s. (a) Three distinct regions (labeled A, B, or C) depending on Au to Si ratio. Region A, corresponding to the region with the smallest amount of Si, produces dendrite structures. Region B, corresponding to the region with intermediate Si concentration, shows rectangular structures. Region C, corresponding to the region with the highest Si concentration, shows the agglomeration of Au-Si mixture on the Si surface. (b) Rectangular structures in Region B shown at higher resolution. (c) TEM image of the edge of a rectangular structure in which stereomicroscopy was done to inform the schematic shown. (d)–(f) HAADF STEM images of a rectangle structure. Z-contrast imaging used to map locations of (e) Au and (f) Si showing that the region outside the rectangle is dominantly Si whereas Au primarily lies on the edge of the rectangle as well as the dark features within the rectangle

The resulting microstructure of low Si concentrations (Region A) was further investigated using the unique sample geometry of the microfabricated sample, a SEM image of which is shown in **Fig. 7**a. The resulting structures, shown in the TEM micrographs in **Fig. 7**b-d and **Fig. 8**, varied depending on temperature. **Fig. 7**b [35] illustrates the

microstructure of the microfabricated device heated just to the eutectic temperature and then immediately cooled. The microstructure consists mostly of Au-Si dendritic structures with 'fractal-like' structures that appear near the edge of the free-standing Au portion of the microfabricated samples. Presumably, these dendrite structures nucleated from Si islands not completely removed from these regions during the Bosch etching process. The region within the dotted box in **Fig. 7**b is shown in more detail in **Fig. 7**c. Here, it is clear to see the Au-Si dendrites as well as the unreacted Au film directly ahead of the reaction front. At this temperature, the dendrite branches do not reconnect and form islands larger than Au grains. The white regions are the non-native SiO_2 layer in which the dark Au-Si mixture formed upon. The microstructure shown in further detail in **Fig. 7**d clearly shows the regions where the Au-Si mixture formed, the remaining unreacted Au film, and the silicon oxide base layer (each labeled). With this sample configuration (limited Si available), only a portion of the Au film reacts with Si, which leaves Au and Au-Si remaining on the SiO_2 layer after cooling.

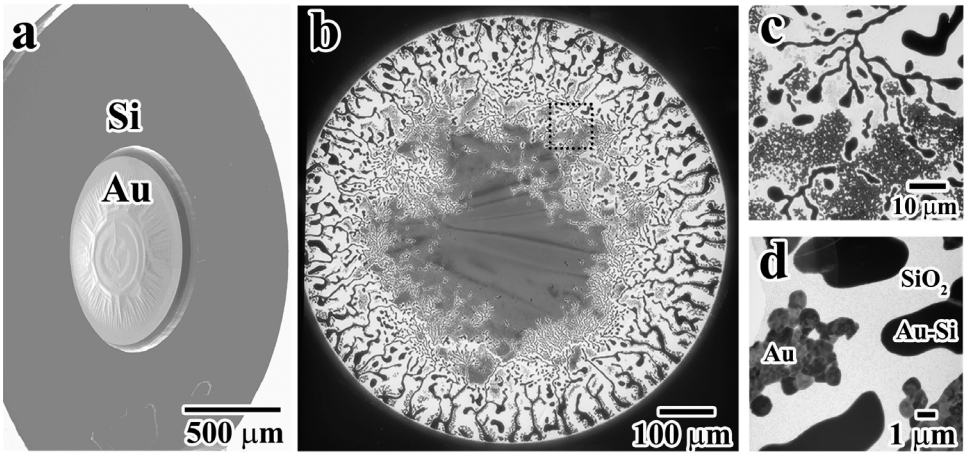

Fig. 7 Resulting microstructure of microfabricated devices after heating to the eutectic temperature and immediately cooled. (a) SEM micrograph of microfabricated TEM sample that provides a 1 mm diameter free-standing Au film supported by 3mm outer diameter silicon washer. TEM micrographs of (b) - (d) the dendrite structure resulting from heating just to the eutectic temperature shown at different magnifications

Alternatively, when samples were heated to temperatures significantly above the eutectic temperature, the free-standing Au film completely reacts to form a complex gold silicide structure on a silicon oxide film. This is shown in **Fig. 8** for a microfabricated sample heated to 873 K. The black region is the gold silicide while the white region is once again a silicon oxide film on top of which the Au-Si mixture (gold silicide) forms. The additional heating led to dendrite coarsening and complex closed-loop 'fractal-like' formations (reconnected branches), which is better seen in **Fig. 8**b. These structures connect to the larger gold silicide in the center of the sample and presumably, the dendrite

structures formed first before the full Au film was convereted at these elevated temperatures.

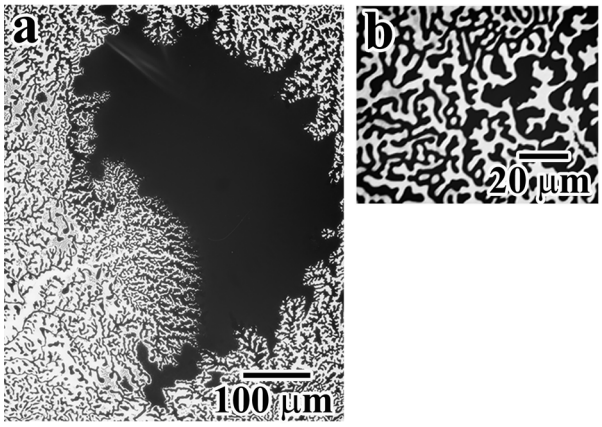

Fig. 8 TEM micrographs of microfabricated sample heated above the eutectic temperature to 873K. This resulted in (a) full conversion of the Au film and a complex 'fractal-like' structure, (b) detailed structure of the coarsening 'fractal-like' dendrites

The post-mortem structure of the eutectic reaction was further investigated by analyzing the cross-section microstructure. Analysis of the resulting microstructure from the *in situ* heating experiment detailed in **Fig. 3** can be seen at lower magnification in **Fig. 9**. The microstructure consists of a completely reacted large grained gold silicide layer (Area 1) on top of an unreacted silicon film. There is also a surface diffusion path along the Si in which the mixture has progressed 6.5 µm from the initial Au film (Area 2). Diffraction analysis of the converted film reveals the structure is closest to Au_5Si_2, which has been suggested as one of the many metastable gold silicide forms [10].

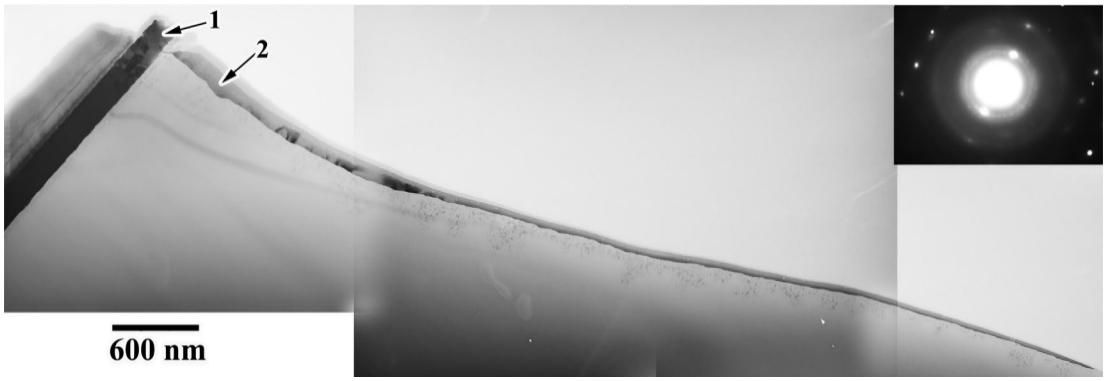

Fig. 9 TEM micrograph of the resulting microstructure from the Au-Si eutectic reaction investigated in cross-section in Fig.3. Complete conversion of the Au film occurred (Area 1). The eutectic mixture diffused over 6.5 µm along the free surface (Area 2). The single crystal diffraction pattern is that from the transformed film in Area 2

3. Discussion

a. Dynamics of the Au-Si eutectic reaction at limited dimensions

This study has shown that the Au-Si eutectic reaction is a complex process and that the final bond structures are a result of an intricate evolution of the microstructure. This evolution first involves the motion of lattice dislocations and grain boundaries within the Au film as the annealing begins which can be seen by comparing initial microstructure (**Fig. 1**a) and the microstructure after sufficient heating (**Fig. 2**a). This is shortly followed by diffusional processes, including Si diffusion along the grain boundaries (seen in **Fig. 5**). Once the eutectic temperature is reached, the Au-Si mixture forms at the Au-Si interface (**Fig. 3**) and penetrates the Au grain boundaries and triple junctions. Far surface diffusion of the liquid Au-Si mixture simultaneously occurrs as seen in cross-section **Fig. 9.** The resulting microstructure has been found to be a function of Au to Si ratio, sample dimensions, and annealing temperature.

The complexity of the eutectic reaction of a Au thin film on a Si substrate differs from classical expectations of eutectic reactions due to the limited dimensions. The observations differ in that the limited geometry introduces an increased number of free surfaces, grain boundaries, and other structural defects to alter the transformation.

Prior to the eutectic reaction, apparent grain growth in the Au films is observed both in plan-view and cross-section. This grain boundary migration occurs after the film has relaxed and lattice dislocations have been removed. Grain growth is commonly observed during annealing and has been previously reported to occur in similar Au thin films heated to 573 K [36], but has not been reported to occur coupled with the eutectic reaction. It is possible that the observed grain boundary migration is driven by both the Si diffusion and thermal activation, as it was found that the Au grain boundaries facilitate diffusion of Si into the Au films prior to the eutectic temperature (seen during *in situ* STEM heating of cross-section in **Fig. 5**). Diffusion-induced grain boundary migration (DIGM) has been previously reported for a wide variety of material systems [37–39], including instances leading to grain growth [40,41]. There are a variety of explanations for DIGM, including boundary migration via self-sustained climb of grain boundary dislocations due to the diffusion of solute species out of the boundary [42], or an overall increase in driving force for boundary migration due to discontinuity in chemical composition across the boundary [43]. Additionally, diffusion of species along grain boundaries have been reported to ‘soften’ the boundaries [44] which could facilitate easier migration.

Once the eutectic temperature is met, the Au-Si mixture penetrates the grain boundaries and converts the boundarties into an interface between the solid Au grains and the liquidous Au-Si mixture. This indicates that the observed grain growth seen in **Fig. 2**a-**Fig**. **2**d is likely a result of the eutectic transformation of the Au film rather

than thermally activated grain growth or DIGM. During this process, the grain size increased at an average rate of 46 nm s^{-1} prior to complete conversion of the Au film at temperatures above the eutectic point (**Fig. 2**a-**Fig**. **2**d). This rate is higher than prevous reports of annealing similar Au films at 573 K which resulted in an average grain size increase at a rate of 9.6 nm s^{-1} [36]. This further indicates that the observed grain growth specifically seen in **Fig. 2** is likely controlled by the penetration of the grain boundaries with the Au-Si liquidous mixture.

Si diffusion into Au during the eutectic bonding process is consistent with previous reports of the diffusion occurring well below the eutectic point [18–21,45]. However, these reports found that the amount of Si diffusion depends on annealing atmosphere, with an air environment promoting increased diffusion. The result presented here based on *in situ* STEM heating (**Fig. 5**) show that Si diffuses into Au readily at low temperatures (593 K) even in a vacuum environment. The initial nanocrystalline nature of these films allow many low energy pathways for Si diffusion to occur at this limited length scale.

Once the eutectic temperature is met, the *in situ* cross-sectional TEM demonstrates the microstructural relaxation of the Au-Si interface that has been evaluated by other methods [27]. This leads to the formation of Au-Si liquidous mixture at the interface, which then penetrates the Au grain boundaries. This is consistent with previous reports of gold silicide formation viewed along Au grain boundaries on the surface of the film [46]. This continues until the last remnants of the Au thin film are rounded islands of Au that are surrounded by the liquidous Au-Si mixture that has thickened grain boundaries and widened triple junctions. The conversion of the Au film was found to occur in a discontinuous fashion with periods of exponential consumption followed by stagnation. The transformation plateaus are likely associated with the exhaustion of diffusion pathways along grain boundaries that limit the transformation. This is also consistent with classic eutectic theory that states that the overall interface velocity will depend on the short-range diffusion of the solute (Si) in the liquid close to the inferface [47].

It is interesting to note that in the cross-section specimens, there is no indication that Au diffuses into the bulk Si directly adjacent to the film, which is contrary to what has been reported in literature both in bulk materials [16] and TEM samples [8,15]. Instead, significant surface diffusion of the Au-Si mixture occurred along the free surface, possibly indicating that this is the preferred mechanisms of Au diffusion at these limited dimensions and free surface availability. Uncontrolled surface diffusion, or overflow, is a common issue reported during MEMS wafer bonding [6]. It is important to control overflow as it can cause failure via electrical shorts and uncontrolled bonding. Lin *et al.* found that decreasing bonding temperature and/or pressure decreased the tendency for overflow [6]. In this study,

surface diffusion was only observed in specimens with an available free surface at the eutectic temperature, which indicates that sample geometry plays an important role. In fact, the Au-Si mixture was found to agglomerate in samples without free-surface availability but similar small Au to Si ratio (Region C in **Fig. 6**a). This indicates that the sample geometry has a large impact on the resulting Au-Si eutectic bond microstructure.

b. Influence of Au to Si ratio on eutectic structure

The resulting structure from the complex dynamics of the transformation is determined by a variety of controlling factors. In this study, the most important factor was found to be the relative ratio of Au to Si. The agglomerated Au-Si mixtures observed on the Si substrate at high Si to Au concentration (Region C in **Fig. 6**a) are expected based on classical eutectic theory. Under this condition, it is likely that the eutectic phase nucleates at the Au-Si interface and grows towards the Au surface. The agglomerates could lead to an inhomogeneous bonding interface and incomplete bonding. This is consistent with previous reports that the Au-Si bond yield decreases with increasing Si concentration [6]. Philofsky *et al.* have reported that these structures can be controlled and manipulated by altering the cooling rate [29]. Attempts were made to determine the effect of quenching rate but were unsuccessful due to brittleness of the supporting oxide layer.

The unique microstructure found in the intermediate Si to Au ratio regime (Region B) is similar to previous reports of square-shaped microstructures. However, in those reports, the square-shape is a result of the epitaxial growth of gold silicide on a (100) Si substrate [16,27–29]. In this study, the rectangular shapes were found to be composed of Au-Si islands supported by a membrane, with a Au-Si ring outlining the rectangle. The remaining portion of the region outside the rectangles is dominantly Si. Based on the stereographic analysis, the membrane is believed to be a thicker silicon oxide layer grown on top of the Au film. This is additional evidence of Si diffusion through the Au film as silicon oxide is formed on the Au film surface. These rectangle structures are possibly a result of both agglomeration and thermal Si etching from heating above the eutectic temperature. This would suggest that Au or Au-Si mixture promotes thermal etching of Si at temperatures below that which it typically occurs [48]. Alternatively, the rectangular features could be Kirkendall voids that form due to unequal interdiffusion between Au and Si [49]. These would be caused by Si diffusion out of these regions into the Au film and can also indicate different diffusion ratios along various Si directions and that there is likely a preferred diffusion direction. Once again, the inhomogeneous nature of this microstructure could lead to inefficient eutectic bonding.

The structure in the area of minimal Si concentration (Region A) varies greatly from the previous two regions,

but is similar to that of other eutectic reactions as discussed by Elliott in that typical dendritic structures are formed during the eutectic transformation [47]. There are also many other reports of dendritic structures forming specifically from the Au-Si eutectic reaction [2,27,28]. The dendritic structure was further investigated with the microfabricated specimens and was found to depend heavily on the heating condition. When heated only to 636 K and immediately cooled, the sample exhibited simple dendritic structures and incomplete transformation of the Au film. If the sample was heated above the eutectic point, a complex dendritic pattern emerged along with complete conversion of the Au film. The patterns coarsened when annealed at temperatures above the eutectic temperture, resulting in those seen in **Fig. 8**b. Similar results obtained by Sekar *et al.* were classified as fractals with an average dimension of 1.69 [26]. There are multiple studies that claim stronger bonding is achieved as the bonding temperature increases past the eutectic temperature [2,4]. The dendrite coarsening and complete conversion of Au film in this study can explain the observed increase in bond strength as the bonding temperature increases. However, it is important to note that increasing the temperature may damage temperature-sensitive devices and is not always a viable option to improve bonding strength.

The unique 'fractal-like' dendrite patterns observed in the microfabricated specimens is due to the Au-Si mixture flowing on top of the thin silicon oxide layer. The contours of this layer may play a substantial role in the directionality and velocity of the Au-Si liquid flow. No substantial change in the dendrite pattern was observed as the heating and cooling rate varied.

The variety of microstructures and instability of the Au/Si interface has posed many challenges to the Si based electronics and MEMS industries. The highly depressed eutectic temperature (636 K) relative to the Au (1063 K) and Si (1412 K) melting temperature limits the operation temperature range for many electronic devices without a diffusion barrier. This temperature range is further depressed due to the instabilities of metastable gold silicide formation. This study suggests that factors such as grain size could play an important role in the eutectic bonding process by providing additional diffusion pathways as the grain size decreases. This paper provides some insight into the fundamental dynamics of these instabilities, which may aide in the design and processing of diffusion barrier and other methods to improve devices dependent on these interfaces.

4. Conclusion

This study offers an in-depth view of the mechanisms and resulting microstructure of the Au-Si eutectic reaction documented using *in situ* TEM and STEM heating experiments for samples of different geometries. Below the eutectic

temperature, significant relaxation of the Au film occurs, including the removal intragranular dislocations. This is followed by a short recrystallization period leading to grain growth of Au film. At the eutectic temperature, a liquidous mixture of Au-Si forms and penetrates the Au grain boundaries. Significant surface diffusion of the Au-Si liquidous mixture occurs for sample geometries with available free surface. The resulting eutectic microstructure was largely found to be a function of Si concentration and heating temperature. As the ratio of Au to Si decreased, the resulting microstructure varied from Au-Si dendrites to rectangular structures and finally to Au-Si agglomerates for the largest Si concentration. Samples heated above the eutectic temperature showed complete conversion and coarsened dendrites.

5. Materials and Methods

The evolution of the microstructure during the Au-Si eutectic reaction was investigated through *in situ* TEM heating of electron transparent Au thin films supported on a Si substrate using both diffraction contrast and STEM imaging modes. Three different sample geometries (traditional plan-view, traditional cross-sectional, and microfabricated plan-view samples) were used in this study, with the geometry of each shown in **Fig. 10**. For each of the geometries, Au films were sputter deposited on a 350 μm-thick prime grade double-side-polished

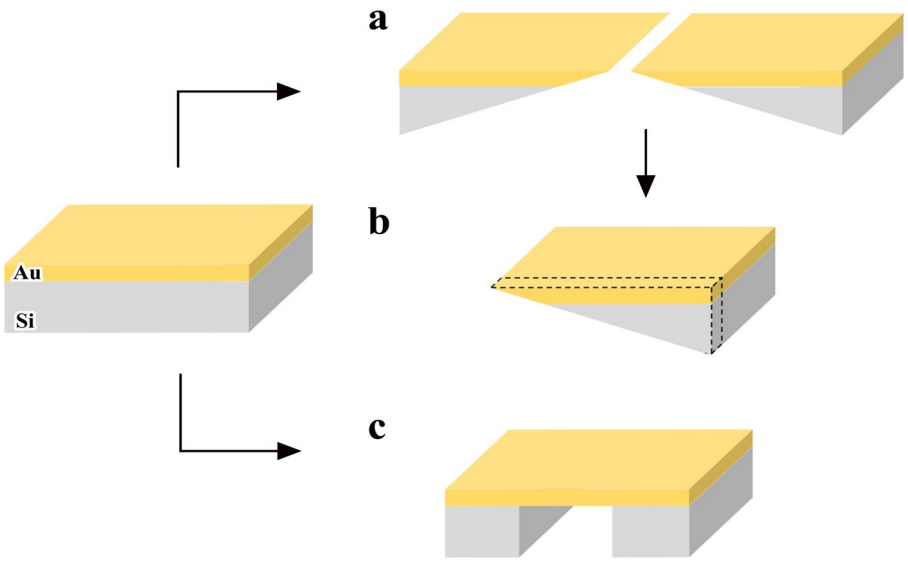

Fig. 10 Schematic of the three different sample geometries. (a) Traditional plan-view, (b) traditional cross-sectional sample (the dashed lines represent cross-section cut), (c) microfabricated sample with Si etched from the backside. All samples were fabricate starting with Au sputter deposited on Si substrate.

Si wafer with a <100> orientation from a 99.99% pure target at 80 W and at a base pressure of 10^{-6} Torr. The film thicknesses were either 100 or 200 nm. The natural oxide layer on the wafer was reduced by immersing the wafer in buffered hydrofluoric acid and cleaned with deionized water prior to Au deposition.

Traditional plan-view samples (**Fig. 10**a) were prepared at room temperature using a backside etching preparation technique utilizing a Dimpler and Gatan Precision Ion Polisher System (PIPS), which resulted in an unknown variation of Au to Si ratio in the electron transparent region. Traditional cross-sectional samples (**Fig. 10**b) were prepared using a common TEM sample preparation technique that included dicing the Au coated wafer, adhering the two Au faces using M-bond and then creating an electron transparent region via dimpling and PIPS milling [34]. The maximum temperature was 293 K for this process. A microfabrication method was used to produce a uniformly thick, electron transparent, free-standing Au window supported and anchored to a 350 μm-thick Si washer (**Fig. 10**c and **Fig. 7**a) for large area plan-view observation. This structure was produced by patterning and etching the backside of the Au coated Si wafer. A single etch of the Si was performed using the Bosch process in an inductively coupled plasma deep reactive-ion etching (ICP-DRIE) chamber [50]. The microfabrication process required temperatures up to 363 K for less than ten minutes. The combination of these three sample geometries allowed for an in-depth analysis of the complex Au-Si eutectic reaction.

The *in situ* TEM heating experiments were performed on a JEOL 4000 TEM operating at either 300 or 350 kV depending on sample thickness. The *in situ* STEM heating experiments were preformed using high angle annular dark field (HAADF) imaging on a JEOL 2010EF STEM microscope operating at 200 kV. *In situ* heating was done using a Gatan heating stage with an accuracy of ±2 K as determined by the eutectic reaction. The samples were heated at various rates ranging from 1 K/min to 20 K/min. The extent of the eutectic reaction can be controlled and studied in depth by bringing the global temperature of the sample to slightly below the eutectic and using local electron beam heating to induce the reaction. Post-mortem chemical mapping of the resultant structures via energy dispersive X-ray spectroscopy (EDX) analysis was performed in either a VG 501 dedicated STEM or on a Philips CM12 TEM. Stereomicroscopy was also performed on a JEOL 4000 TEM.

6. Acknowledgements

The authors would like to acknowledge Drs. J.A. Dantzig, L. H. Allen, A. W. Hubler, J. E. Greene, T.A. Saif, and J. H. Han.

7. Declarations

Funding. This research was funded by NSF DMR award # 02037400. S.S. is supported by the U.S. Department of Energy (DOE) National Nuclear Security Administration (NNSA) Stewardship Science Graduate Fellowship (SSGF) program, provided under cooperative agreement number DE-NA0003960. Microscopy presented in this work was performed in the Center for Microanalysis of Materials at the University of Illinois which is partially supported by the U.S. Department of Energy under grant DEFG02-91-ER45439 and by the University of Illinois. K.H. was supported by the DOE-BES Materials Science and Engineering Division under FWP 15013170. This work was performed, in part, at the Center for Integrated Nanotechnologies, an Office of Science User Facility operated for the U.S. Department of Energy (DOE) Office of Science. Sandia National Laboratories is a multimission laboratory managed and operated by National Technology & Engineering Solutions of Sandia, LLC, a wholly owned subsidiary of Honeywell International, Inc., for the U.S. DOE's National Nuclear Security Administration under contract DE-NA-0003525. The views expressed in the article do not necessarily represent the views of the U.S. DOE or the United States Government.

Conflict of interest. The authors have no relavant financial or non-financial intersts to disclose.

Availability of data and material. No datasets were generated or analyszed during this study.

Code availability. Not applicable

8. References

[1] K. Zhu, C. Wen, A.A. Aljarb, F. Xue, X. Xu, V. Tung, X. Zhang, H.N. Alshareef, M. Lanza, Nat. Electron. 4 775–785 (2021).

[2] D. Li, Z. Shang, Y. She, Z. Wen, Micromachines. 8 (2017).

[3] Y.T. Cheng, L. Lin, K. Najafi, J. Microelectromechanical Syst. 9 3–8 (2000).

[4] S.M.L. Nai, J. Wei, P.C. Lim, C.K. Wong, Proc. 5th Electron. Packag. Technol. Conf. EPTC 2003. 119–124 (2003).

[5] J. Wu, Y.-L. Shen, K. Reinhardt, H. Szu, B. Dong, Appl. Comput. Intell. Soft Comput. 2013 1–13 (2012).

[6] Y.C. Lin, M. Baum, M. Haubold, J. Frömel, M. Wiemer, T. Gessner, M. Esashi, Development and evalution of AuSi eutectic wafer bonding, in: Transducers, 2009: pp. 244–247.

[7] M.S. Ashtikar, G.L. Sharma, J. Appl. Phys. 34 5520–5526 (1995).

[8] P.H. Chang, G. Berman, C.C. Shen, J. Appl. Phys. 63 1473–1477 (1988).

[9] G.A. Andersen, J.L. Bestel, A.A. Johnson, B. Post, Mater. Sci. Eng. 7 83–90 (1971).

[10] B.Y. Tsaur, J.W. Mayer, Philos. Mag. A. 43 345–361 (1981).

[11] C. Suryanarayana, T.R. Anantharaman, Mater. Sci. Eng. 13 73–81 (1974).

[12] L. Hultman, A. Robertsson, H.T.G. Hentzell, I. Engström, P.A. Psaras, J. Appl. Phys. 62 3647 (1998).

[13] T.R. Anantharaman, H.L. Luo, W. Klement, Nature. 210 1040–1041 (1966).

[14] F.H. Baumann, W. Schroter, Phys. Rev. B. 43 6510–6510 (1990).

[15] M. Terauchi, N. Umemoto, Y.K. Sato, M. Ageishi, A.-P. Tsai, Microscopy. 00 1–7 (2021).

[16] L. Lin, Y.T. Cheng, K. Najafi, Jpn. J. Appl. Phys. 37 (1998).

[17] H. Liang, B. Xiong, Semicond. Sci. Technol. 35 (2020).

[18] A.K. Green, E. Bauer, J. Appl. Phys. 47 1284 (1976).

[19] A. Hiraki, E. Lugujjo, J.W. Mayer, J. Appl. Phys. 43 3643–3649 (1972).

[20] N. Sumida, K. Ikeda, Ultramicroscopy. 39 313–320 (1991).

[21] C. Chang, G. Ottaviani, Appl. Phys. Lett. 44 901–903 (1984).

[22] A. Cros, C. Canella, J. Adhes. Sci. Technol. 5 1041–1048 (1991).

[23] M. Seibt, S. Buschbaum, U. Gnauert, W. Schröter, D. Oelgeschläger, Phys. Rev. Lett. 80 774–777 (1998).

[24] M. Paulosem, O.K. Varghese, C.A. Grimes, J. Nanosci. Nanotechnol. 3 341–346 (2003).

[25] D. Hourlier, P. Perrot, Mater. Sci. Forum. 653 77–85 (2010).

[26] K. Sekar, G. Kuri, P. V. Satyam, B. Sundaravel, D.P. Mahapatra, B.N. Dev, Solid State Commun. 96 871–875 (1995).

[27] B. Bokhonov, M. Korchagin, J. Alloys Compd. 312 238–250 (2000).

[28] H. Kato, Jpn. J. Appl. Phys. 28 953 (1989).

[29] E. Philofsky, K. V. Ravi, J. Brooks, E. Hall, J. Electrochem. Soc. 119 527 (1972).

[30] G.D. Hibbard, K.T. Aust, U. Erb, J. Mater. Sci. 43 6441–6452 (2008). https://doi.org/10.1007/S10853-008-2975-5/FIGURES/12.

[31] J. Kacher, I.M. Robertson, M. Nowell, J. Knapp, K. Hattar, Mater. Sci. Eng. A. 528 1628–1635 (2011). https://doi.org/10.1016/J.MSEA.2010.10.109.

[32] P.X. Yan, J. Chang, W.L. Wang, X.N. Zhu, M.J. Lin, B. Wei, Acta Mater. 237 118149 (2022). https://doi.org/10.1016/j.actamat.2022.118149.

[33] Z.C. Luo, C.H. Zheng, H.P. Wang, Mater. Charact. 186 111776 (2022). https://doi.org/10.1016/J.MATCHAR.2022.111776.

[34] D.B. Williams, C.B. Carter, Transmission Electron Microscopy, 2nd ed., Springer Science & Business Media, 2009.

[35] K. Hattar, Mater. Today. 9 (2006).

[36] K.M. Hattar, Thermal and Mechanical Stability of Nanograined FCC Metals, University of Illinois at Urbana-Champaign, 2009.

[37] Z. Shen, K. Arioka, S. Lozano-Perez, Corros. Sci. 183 109328 (2021).

[38] K. Tashiro, G.R. Purdy, Scr. Metall. 21 361–364 (1987).

[39] D.B. Butrymowicz, D.E. Newbury, D. Turnbull, J.M. Cahn, Scr. Metall. 18 1005–1010 (1984).

[40] H. Stange, S. Brunken, D. Greiner, M.D. Heinemann, C.A. Kaufmann, S.S. Schmidt, J.P. Bäcker, M. Klaus, C. Genzel, R. Mainz, Acta Mater. 111 377–384 (2016).

[41] I.I. Danzo, Y. Houbaert, K. Verbeken, Surf. Coatings Technol. 251 15–20 (2014).

[42] R.W. Balluffi, J.W. Cahn, Acta Metall. 29 493–500 (1981). https://doi.org/10.1016/0001-6160(81)90073-0.

[43] M. Hillert, Scr. Metall. 17 237–240 (1983). https://doi.org/10.1016/0036-9748(83)90105-9.

[44] S. Yu, D.J. Siegel, ACS Appl. Mater. Interfaces. 10 38151–38158 (2018). https://doi.org/10.1021/acsami.8b17223.

[45] A. Hiraki, M. Nicolet, J.W. Mayer, Appl. Phys. Lett. 18 178–181 (1971).

[46] S. Mathot, G. Demortier, Nucl. Instruments Methods Phys. Res. Sect. B. 226 222–230 (2004).

[47] R. Elliott, Eutectic solidification processing, 1983.

[48] A. Reisman, S.T. Edwards, P.L. Smith, J. Electrochem. Soc. 135 2848 (1986).

[49] B. Selikson, Proc. IEEE. 57 1594–1598 (1969). https://doi.org/10.1109/PROC.1969.7341.

[50] C. Chang, Y.-F. Wang, Y. Kanamori, J.-J. Shih, Y. Kawai, C.-K. Lee, K.-C. Wu, M. Esashi, J. Micromechanics Microengineering. 15 580–585 (2005).